Revealing the Complexity of Heterogeneous Volcaniclastic Facies of Mid Miocene Onnagawa Formation, Akita Basin, Japan*

Ivan Zhia Ming Wu[1], Sarvagya Parashar[1], M.S Iyer[1], Chung Yee Lee[1], Hideo Komatsu[2], and Saki Shimada[2]

Search and Discovery Article #11175 (2019)**
Posted January 14, 2019

*Adapted from extended abstract prepared in conjunction with oral presentation given at 2018 International Conference and Exhibition, Cape Town, South Africa, November 4-7, 2018
 DOI:10.1306/11175Wu2019

[1]FRS, Halliburton, Kuala Lumpur, Kuala Lumpur, Malaysia (Ivanzhiaming.wu@halliburton.com)
[2]Inpex, Akita, Japan

Abstract

Volcanic rocks exhibit numerous variations of features that reflect the complexity associated with volcanic edifices. This study consists of heterogeneous lithocolumns that must be evaluated with a high-resolution textural analysis to derive a reliable lithofacies model.

A detailed analysis of high-resolution images was used to define the associated lithofacies and morphofacies of the drilled lithocolumn. This methodology can be broadly categorized in three major steps. The first step includes the identification of the image electrofacies using the processed microresistivity borehole images and dips, supplemented by observations from open hole logs, geochemical logs, and mud log descriptions. In the second step, the recognized subfacies are interpreted in terms of depositional processes and conditions. The third step groups the identified subfacies into distinct facies associations, which are predictors of certain depositional settings. After the successful characterization of image-based electrofacies, an integrated approach was adopted to link the various facies with elemental spectroscopy data to identify the relationship between the genesis and emplacement of various rock types.

In the study well, the facies can be grouped into five major sections: FA1, FA2, FA3, FA4, and FA5. The basal section, FA1 of the study interval, is primarily characterized by explosive facies, consisting of base surge and pyroclastic deposits. FA2 is also dominated by explosive facies, including an increase in calcium feldspar, with reduced potassium feldspar and very low clay content across the extrusive facies interval. FA3 is characterized by a massive unit rich in calcium feldspar, dolomite, and pyroxene. The upper section of the study well, represented by FA4, is silica-rich at the bottom and magnesium-calcium-rich. This interval is characterized by the mixing of reworked volcanogenic sedimentary facies with extrusive facies. The uppermost part of the entire interval is represented by FA5 which is silica- and clay-rich, with strong evidence of potassium feldspar. These identified facies were analyzed in the holistic vertical sequence in association with all other

conventional well logs, such as nuclear magnetic resonance (NMR), acoustic, and triple combo, to build an in-depth understanding of the distribution of geological facies in the major volcanic edifices.

Introduction

Substantial consideration has been given to the formation and distribution rules of volcanic reservoirs since volcanic reservoirs were first discovered as unconventional reservoirs. Numerous studies were conducted to understand the characteristics and distributions of volcanic rocks, the eruption mechanism, volcanic edifices structures, volcanic facies and lithologies, pore space structures, properties of hydrocarbon-bearing volcanic reservoirs, and the settings required for hydrocarbon accumulation (Zou et al. 2013).

Recent studies primarily focus on the type and genesis of the reservoir space, diagenetic evolution of the reservoir, and elements that determine the reservoir development. The research toward understanding the mechanism of the volcanic reservoir formation is lacking. Additional attempts on lithology standardization, classification of the lithologies, nomenclature for the volcanic rocks, understanding the evolution of fluid accumulation, and the controlling factors of reservoir development should be made during hydrocarbon exploration in search of promising reservoirs or sweet spots (Zou et al. 2013).

The terminology used in defining volcanic edifice is highly variable. In their publication, “Voluminous Dictionary of Earth Sciences” (2006), Cheng and Wang define volcanic edifice as “…volcanic body or edifice and means all kinds of volcanic landscapes formed on the ground surface during volcanic eruption, including volcanic cone, volcanic dome, volcanic crater, caldera, and lava plateau; sometimes it also refers to substructures such as volcanic neck, volcanic conduit, etc.…”. Several definitions were also given by other authors, as described by Zou et al. (2013). The grouping of volcanic edifice categories is rather disordered, resulting in variations of shapes and scales (Zou et al. 2013).

Although variations exist in the terminologies used, the terminology used is generally quite similar. Some researchers, however, place more emphasis on the occurrences and shape, whereas others emphasize the lithofacies assemblages. Usually defined as the volcanic activity architecture at given environments, volcanic facies affect the porosity and permeability of volcanic reservoirs directly and become the primary reason for reservoir heterogeneity. With different authors, the categorizations of volcanic facies are not uniform (Zou et al. 2013). In the present case study, the volcanic facies are categorized into volcanic conduit facies, explosive facies, effusive facies, extrusive facies, and volcanogenic sedimentary facies.

Located in the northeastern area of Honshu Island of Japan, the Miocene Onnagawa Formation in the Akita Basin forms a part of the circum-Pacific belt of Neogene diatomaceous sediments (Aoyagi and Iijima 1983), extending from the western side of North America across the present North Pacific Ocean to Japan. The geological age of this formation is estimated to be late middle Miocene; consequently, it is correlatable with parts of the Monterey Formation in California (Kamitsuji et al. 2013). The geological correlation of the Neogene-Quaternary units in northeastern Honsu (Table 1) are such that the northern part ranges toward the northeast from Niigata to Yamagata and Aomori. The lower part of the Teradomari Formation, Kusanagi Formation, and Daidoji Formation are considered to be equivalent to the Onnagawa Formation of Akita prefecture (Aoyagi and Iijima 1983). Figure 1 shows the location of several oil and gas fields of Akita, Japan.

The Onnagawa Formation in Akita consists primarily of hard mudstone, siliceous shale, diatomaceous mudstone, and acidic pyroclastic rocks (Aoyagi and Iijima 1983). Lenses of marl stone are occasionally found in mudstone and shale. The typical siliceous rocks in the Miocene can be recognized only in the southwest of Hokkaido and in the northeast of Honshu (Iijima and Tada 1981). The Onnagawa Formation generally contains planktonic foraminifera, benthonic foraminifera, and diatoms, as reported by Maiya (1978), which points toward bathyal deposition with a low oxygen water column affected by cold oceanic currents.

Although the precise geological age of the formation has not yet been clarified, the foraminiferal assemblages suggest that the formation is of late middle Miocene age, approximately between 12 and 13 Ma in the planktonic foraminiferal N 11-13 zone (Aoyagi and Iijima 1983). Consequently, the Onnagawa Formation can be correlated to the lower section of the Monterey Formation, which was reported with an age of 4.5 to 15 Ma (equivalent to N 9-18 zone) by U.S. Department of the Interior (1978).

Methodology

A sedimentological analysis was performed over a drilled section of sediments approximately 700 m thick in the studied well. Evolutionary steps involved the identification of the image electrofacies using the processed microresistivity borehole images and dips supplemented by observations from open hole logs, geochemical logs, and mud log descriptions. The recognized subfacies are interpreted in terms of depositional processes and conditions. Subsequently, these subfacies are grouped into distinct facies associations, which are predictors of certain depositional settings.

In the present well, the microresistivity image data were analyzed; each facies type was defined using dynamic images and image-derived formation dip results. Dynamic images involve a process that enhances any variations between resistive and conductive features. Consequently, these images help to identify internal sedimentary structures, such as crossbedding and flat lamination. In addition, various image filters are available to facilitate feature recognition. Conventional open hole logs and mud logs are referenced to further support facies identification.

Nine image-based electro-subfacies types have been recognized in the study well interval. The electro-subfacies classification is based on combined image log interpretation, open hole log responses, and geochemical log and mud log descriptions. Figure 2 through Figure 10 show the recognized image facies. Table 2 provides the characteristics of each facies type and their typical mode of formation.

Results and Discussion

In the studied well, the facies can be primarily grouped into five sections: FA1, FA2, FA3, FA4, and FA5. The basal part, FA1 of the study interval, is primarily characterized by explosive facies with potassium feldspar-rich with relatively low calcium and magnesium interval, with major subfacies of base surge deposits and pyroclastic flow deposits. FA2 is also dominated by explosive facies, but extrusive facies is also evident. This interval shows an increase in calcium feldspar with reduced potassium feldspar and very low clay across the extrusive facies interval. FA3 is characterized by a massive unit rich in calcium feldspar, dolomite, and pyroxene with low clay content. An abundance of fractures is exhibited across this interval, indicating a more basaltic origin, which is identified as conduit facies. FA4, the upper section of the study well, is silica-rich at the bottom and magnesium-calcium-rich toward the top. This interval is characterized by the intermixing of a

reworked volcanogenic sedimentary sequence and extrusive facies. The uppermost part of the interval, FA5, is silica- and clay-rich with evidence of potassium feldspar distribution. This interval indicates reworked volcanogenic sedimentary facies (Figure 11).

Facies Associations: 1 (Zone 5)

On a broader geological aspect, the bottom-most part of the section is primarily represented by explosive facies of two major subfacies: base surge deposits and pyroclastic flow. The lower body is represented by image facies of base surge deposit characterized by low to medium magnitude dips (15 to 35 degrees) oriented toward the southwest. It also includes sporadic occurrences of partially open and resistive fractures, with higher fracture density toward the upper section with low gamma ray response (Figure 11). The overall image texture appears to be layered. Some of the beddings seem to be deformed, which contributes to the local deformation within the zone. This lower zone is dominated by base surge deposits exhibiting 67.6% facies distribution, followed by 32.2% of pyroclastic flow deposits. Some highly resistive patches and streaks are also visible in this section, which are associated with mineralogical changes within the entire sequence dominated by the presence of calcium.

Facies Associations: 2 (Zone 4)

Geologically, the section is represented by dominantly extrusive and explosive facies. Interlayering of these facies has been observed at various depths, which is characterized based upon the morphological and textural variations within these subfacies with a major dominance of base surge deposits (36.9%), pyroclastic flow (26.0%), middle extrusive (17.7%), outer extrusive (10.7%), followed by air fall deposits (4.7%). The interval of XX17 to XX20 m appears to be slightly brecciated, exhibiting resistive patches and distorted bedding along with soft sediment deformation at XX17.5 m. Below this interval, two massive units appear to exist with a distinct boundary at XX29.6 m. The unit above this boundary appears to be more conductive and featureless, with some bedding at the base; the lower unit consists of a more resistive host rock with fractures of 50 degrees magnitude with a strike toward the north and northeast. Microresistivity imagery shows a massive interval from XX84 to XX99 m. No beddings and fractures are visible, and it is almost featureless. The interval from XX53 to XX58.5 m appears to be massive, with some welded material appearing as small resistive fragments. A few bright resistive streaks are evident at XX74.8 m and XX77.9 m, with a rounded nodule at XX80.7 m. The microresistivity image appears to be brecciated with a mixture of rocks bound together, with some indications as probable resistive vesicles (XX63 to XX65 m). Rounded features with variations in size and random distribution in the interval are observed in XX70 to XX72 m, with air fall deposit features identified in XX80 to XX82.5 m. Another interesting feature is indicated in XX31.5 to XX50 m, which seems to be massive and fractured with less clear visible beddings. This interval exhibits conductive banding features with a dip magnitude of 15 to 30 degrees toward the south and seems to be almost “rhythmic” with consistent thicknesses (XX41 to XX45 m). The interval of XX20 to XX31.5 m shows the first change of beddings azimuth toward the south-southwest with a magnitude of 10 to 25 degrees. Angular to subangular resistive fragments without beddings are shown on microresistivity images (XX25 to XX30 m). Overall, this interval suggests a consistent dip magnitude that ranges between 10 to 25 degrees oriented toward the south-southwest. This interval also exhibits a boundary of dip reversal from the top section. The smaller drag pattern is visible near the localized fracture zones (XX28 to XX33 m, XX25 m, and XX40 m), and it is dominated by partially open/closed/healed fractures.

Facies Associations: 3 (Zone 3)

Zone 3, from XX70m to XX20m, appears as a massive and resistive body with no evident beddings represented by major intrusive igneous body (sill or dike) with abundant fractures. The upper part of this massive unit is dominated by healed or closed fractures; moving downward, partially open or open fractures are more dominant. The open fracture sets are in a mean strike toward the northwest to southeast direction; the distribution of partial fractures strike ranges from north-northeast to south-southwest. Toward the top, this sequence is represented by explosive breccia characterized by brecciated texture with resistive and conductive patches. Overall, the interval of XX94 to XX20 m exhibits the highest open fracture density in the entire study well.

Facies Associations: 4 (Zone 2)

In Zone 2, from XX70 to XX40 m, the entire interval is dominated by the reworked volcanogenic sediments, interlayered with extrusive facies toward the top and pyroclastic flow toward the bottom. The facies percentage across this interval is dominated by a reworked volcanogenic sedimentary sequence (49%), followed by outer extrusive (31.6%) and middle extrusive (8.3%), with explosive facies represented by air fall deposits, pyroclastic flow, and base surge deposits with 4.1%, 5.2%, and 1.7%, respectively. The extrusive facies predominantly exhibits the presence of fracture sets, giving rise to characteristic dip drag patterns from XX40 to XX03 m. In this region, the increase in dip magnitude from 15 degrees to almost 70 degrees is evident. Angular to subangular fragments and bombs (bright and dark colored) with random orientation are well represented (XX55 to XX60 m) and identified as air fall deposits. These fragments are most likely to be deposited during volcanic eruption-related events, in which the fragments are ejected and fall under gravity and wind influence. The XX60 to XX66.5 m interval appears to be massive, with some indications of fluidal flow with distorted bedding planes, and resistive. These may be deposited as hot volatile mixtures that appear to be massive or welded materials. The basal part of this interval has well preserved parallel beddings with an average of 30 degree magnitude dip toward the southwest. This unit is identified as probable base surge deposits, formed under turbidity flows. The interval from XX82 to XX55 m is primarily characterized by a sedimentary sequence, followed by outer extrusive subfacies. In the sedimentary subfacies, beddings are consistent with dips magnitude ranging from 20 to 70 degrees toward the east. Resistive bands are present, which is well evident from images and open hole logs indicated by the high-density peaks along the interval (XX93 m and XX96 m). Partially closed fractures are concentrated at the upper part (XX82 to approximately XX95 m) in the sedimentary subfacies section, crisscross cutting the bedding planes. This may be attributable to the presence of resistive minerals, which can cause the mechanical properties of the rock to become more brittle and, consequently, more susceptible to development of these fractures. From XX40 to approximately XX82 m, the outer extrusive subfacies is characterized by welded brecciated rock fragments, whereas the middle extrusive subfacies are shown as massive with fluidal indications. Both subfacies have much less beddings preservation. On microresistivity images, it appears to be fractured with an indication of fluid flow and brecciated (for example, XX40 to XX44 m).

Facies Associations: 5 (Zone 1)

Overall, this interval exhibits primarily reworked volcanogenic sedimentary facies at the upper part, overlain by an explosive facies. Subfacies in the interval of XX53 to XX40 m is primarily characterized by a reworked volcanogenic sedimentary sequence (60.6%), followed by pyroclastic flow (34.9%), and some surges of base surge deposits (4.5%). Bedding dips are observed to vary from 2 degrees to approximately

50 degrees magnitude with direction toward the east-southeast. The dip magnitude trend increases from XX53 to approximately XX40 m. For the sedimentary sequence in this section, the bedding dips are consistent and almost parallel, with clear geometry of bedding where the sinusoid can be fitted in almost perfectly. At XX61.2 m, resistive nodules that appear bright in comparison to background resistivity are evident. At XX72.1 m, XX74.2 m, XX78.7 m, XX81.8 m, XX24.7 m, and XX30 m, a few examples of the resistive streaks are evident, which appear to be bright and resistive in microresistivity images. These are features that may be formed as secondary minerals at a later time and distort the image bedding dips and features. Another interesting feature that can also be observed from microresistivity images is the soft sediment deformation structure, which indicates loosely packed sediments. These are well evident across XX10.5 to XX13 m and XX00.8 to XX02 m. The pyroclastic subfacies exhibit an almost consistent bedding trend and appears to be "welded" or more chaotic; however, it still forms a plane geometry with some distortion (for example, in XX99 to XX01 m). Often, it exhibits a pyroclastic structure and may appear as a massive unit. Base surge deposits are represented by parallel beddings. In this interval, the parallel bedding appears to have lower resistivity, resulting in challenges for features identification, but visualization is slightly improved in dynamic images (for example, at XX09 m). A bright resistive streak is also evident at approximately XX86 m, and a xenolith can be observed at XX03.7 m on microresistivity images. This appears to be a rounded resistive nodule that may have a different origin because the beddings drapes across the structure. Overall, no dominant fracture sets are observed in this interval.

Conclusion

This study describes the application of microresistivity images for unconventional reservoirs to identify the textural variations and characteristics to determine the heterogeneity across the volcanics succession. The case study demonstrates the value and importance of using microresistivity images for high-resolution data to identify features for facies classification. Based on the observation and findings, the facies assemblages indicate an explosive facies association toward the lower interval, followed by conduit facies and volcanics-derived sedimentary succession at the top. In addition, the structural information can also be extracted from dips interpretation that can be obtained from microresistivity images; this information helped to reveal the subseismic structural complexity also described in this work.

Acknowledgment

Authors express their sincere appreciation to Inpex Corporation management for permission to publish this study.

References Cited

Aoyagi, K., and A. Iijima, 1983, Reservoir Characteristics and Petroleum Migration in the Miocene Onnagawa Formation of Akita, Japan, *in* C.M. Isaacs, R.E. Garrison, S.A. Graham, and W.A. Jensky II (eds.), Petroleum Generation and Occurrence in the Miocene Monterey Formation, California, Pacific Section: Society of Economic Paleontologists and Mineralogists [now the Society for Sedimentary Geology], Los Angeles, California, May 20–22, 1983, Proceedings, p. 75–84.

Cheng, Y.Q., and H.Z. Wang, 2006, Voluminous Dictionary of Earth Sciences (in Chinese): Geological Publishing House, Beijing, 867 p.

Iijima, A., and R. Tada, 1981, Silica Diagenesis of Neogene Diatomaceous and Volcaniclastic Sediments in Northern Japan: Sedimentology, v. 28, p. 185-200.

Liu, J., P. Wang, Y. Zhang, W. Bian, Y. Huang, H. Tang, and X. Chen, 2012, Volcanic Rock-Hosted Natural Hydrocarbon Resources: A Review: *in* K. Nemeth (ed.), Updates in Volcanology-New Advances in Understanding Volcanic Systems: IntechOpen. doi:10.5772/54587

Kamitsuji, R., S. Yokoi, and T. Okajima, 2013, Acid Stimulation of Onnagawa Tight Oil Formation in Ayukawa Field, Japan: SPE Unconventional Resources Conference and Exhibition-Asia Pacific, Brisbane, Australia, 11-13 November, SPE-167101-MS, 4 p. doi.org/10.2118/167101-MS

Maiya, S., 1978, Late Cenozoic Planktonic Foraminiferal Biostratigraphy of the Oil Field Region of Northeast Japan, *in* K. Fujita, K. Ichikawa, M. Ichihara, M. Chiji, K. Unabara, T. Fujita, and Y. Takayanagi (eds.), Cenozoic Geology of Japan: Osaka city University, p. 35-60 (in Japanese).

U.S. Department of the Interior, 1978, Neogene Biostratigraphy of Selected Areas in the California Coast Ranges, W.O. Addicott (ed.): U.S.G.S. Open File Report 78-446, 109 p.

Zou, C., G. Zhang, R. Zhu, X. Yuan, X. Zhao, L. Hou, B. Wen, and W. Xiaozhi, 2013, Chapter 3 - Characteristics of Volcanic Reservoirs, *in* C. Zou (ed.), Volcanic Reservoirs in Petroleum Exploration: Elsevier, p. 31-90. doi.org/10.1016/B978-0-12-397163-0.00003-8

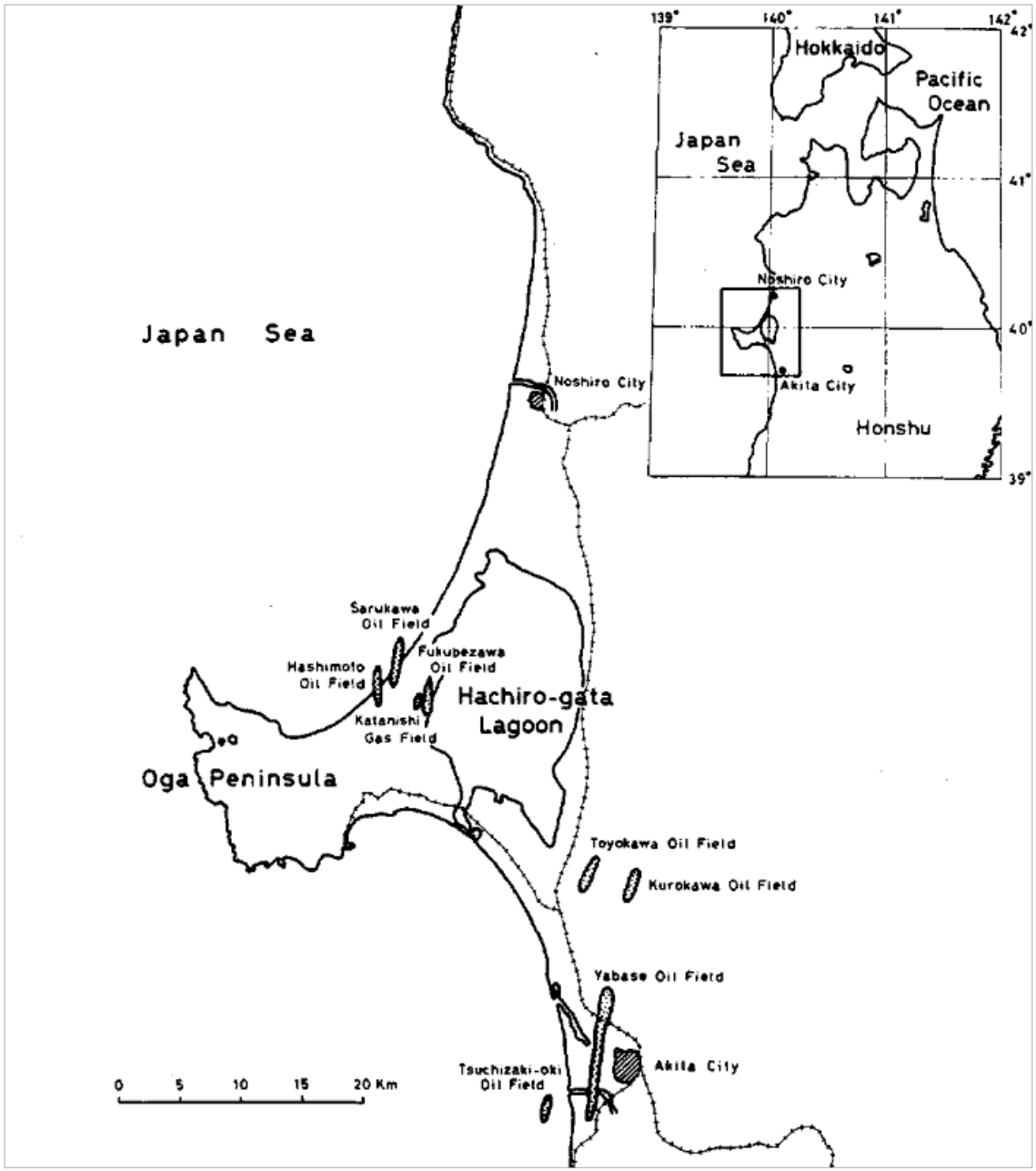

Figure 1. Location map exhibiting various oil and gas fields in Akita, Japan (after Aoyagi and Iijima 1983).

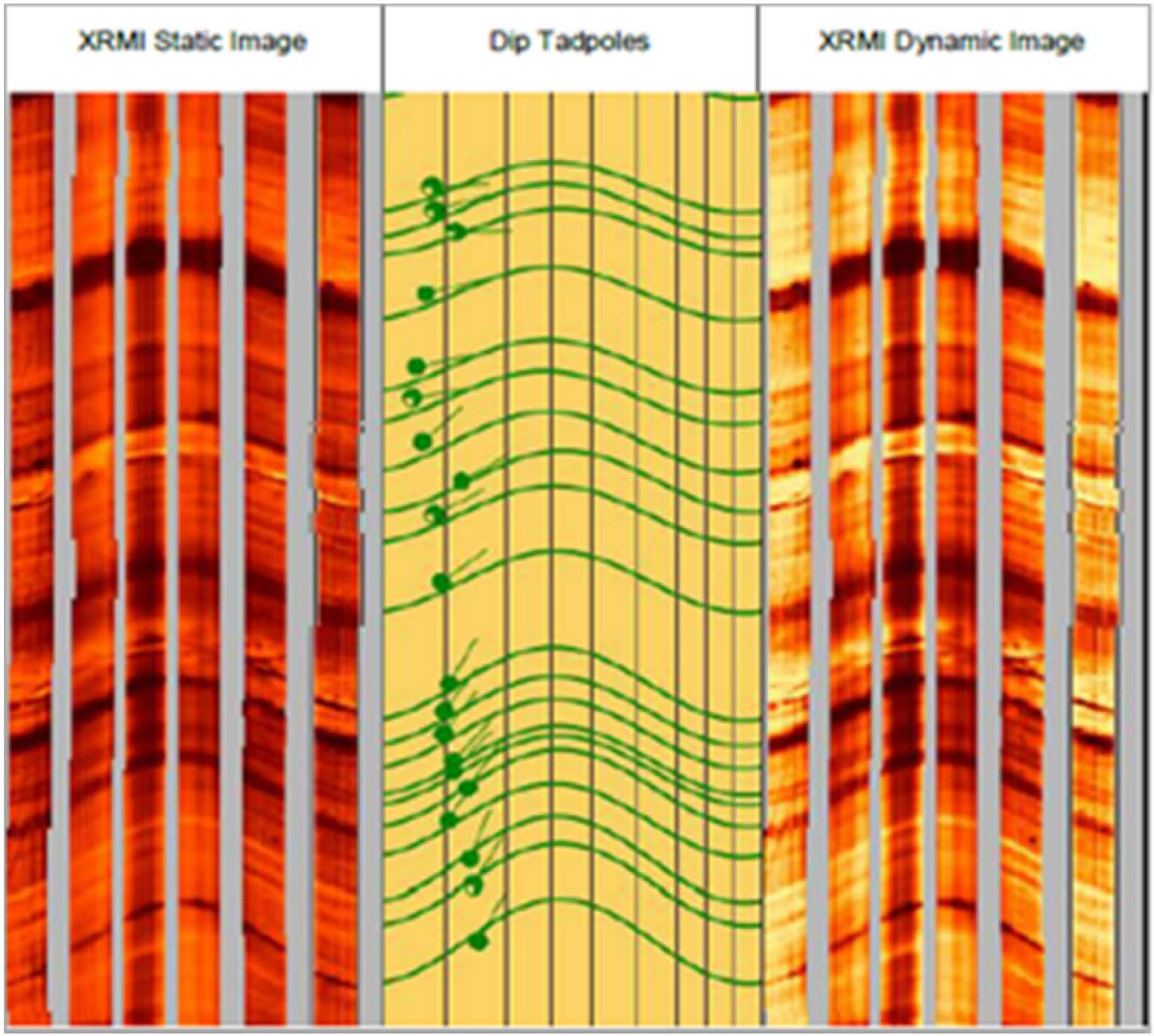

Figure 2. Reworked sedimentary subfacies.

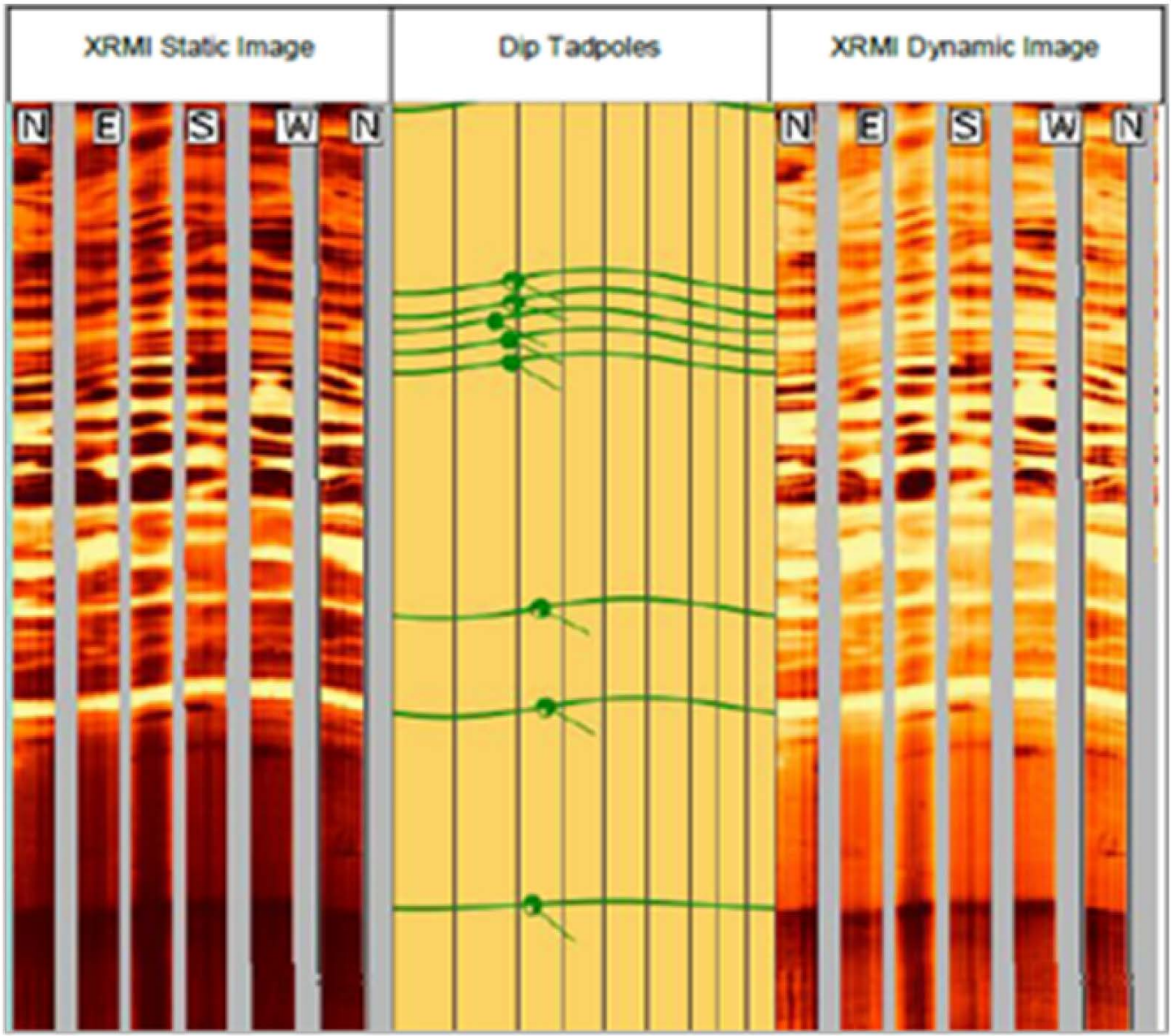

Figure 3. Pyroclastic flow subfacies.

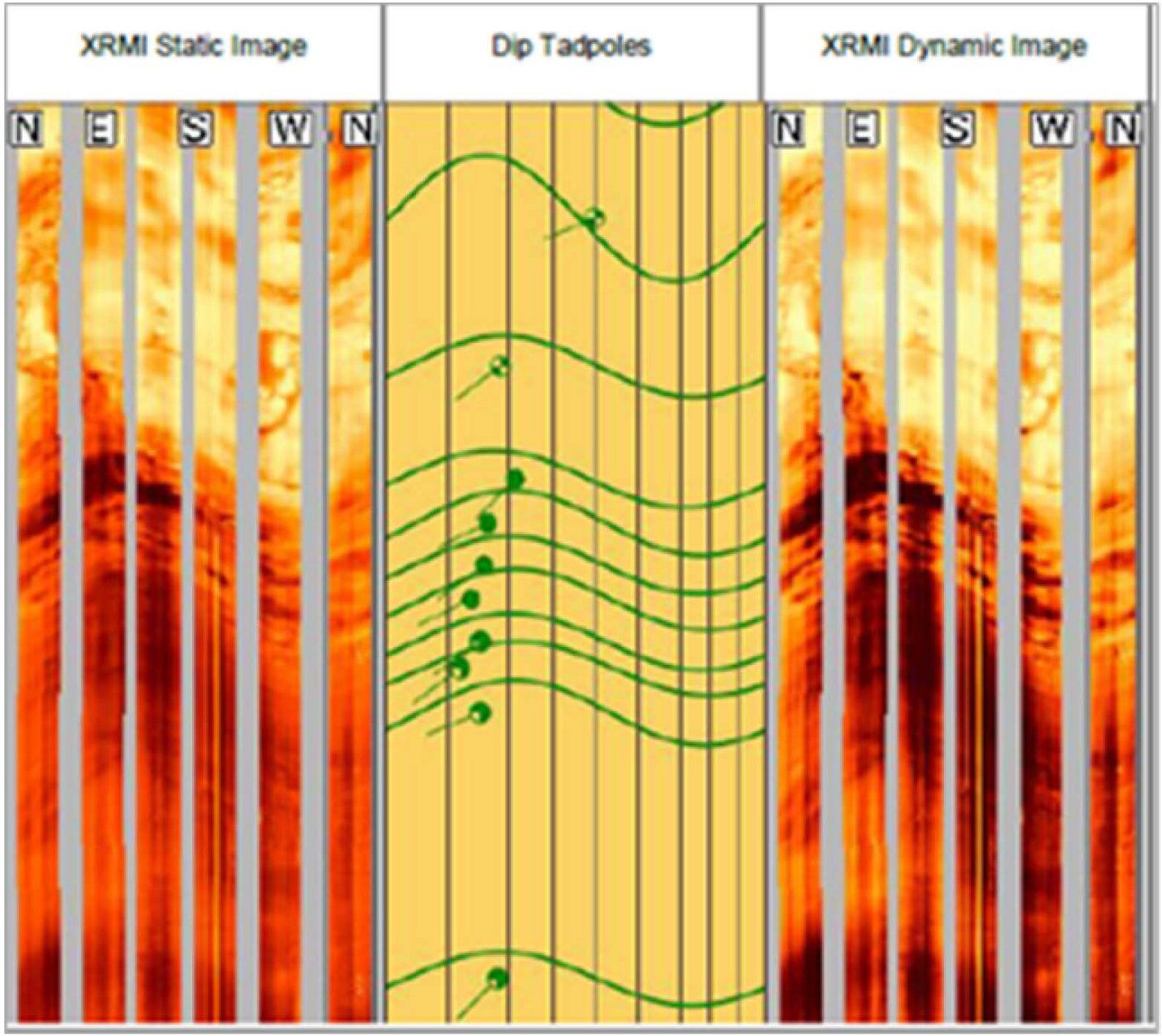

Figure 4. Base surge deposit subfacies.

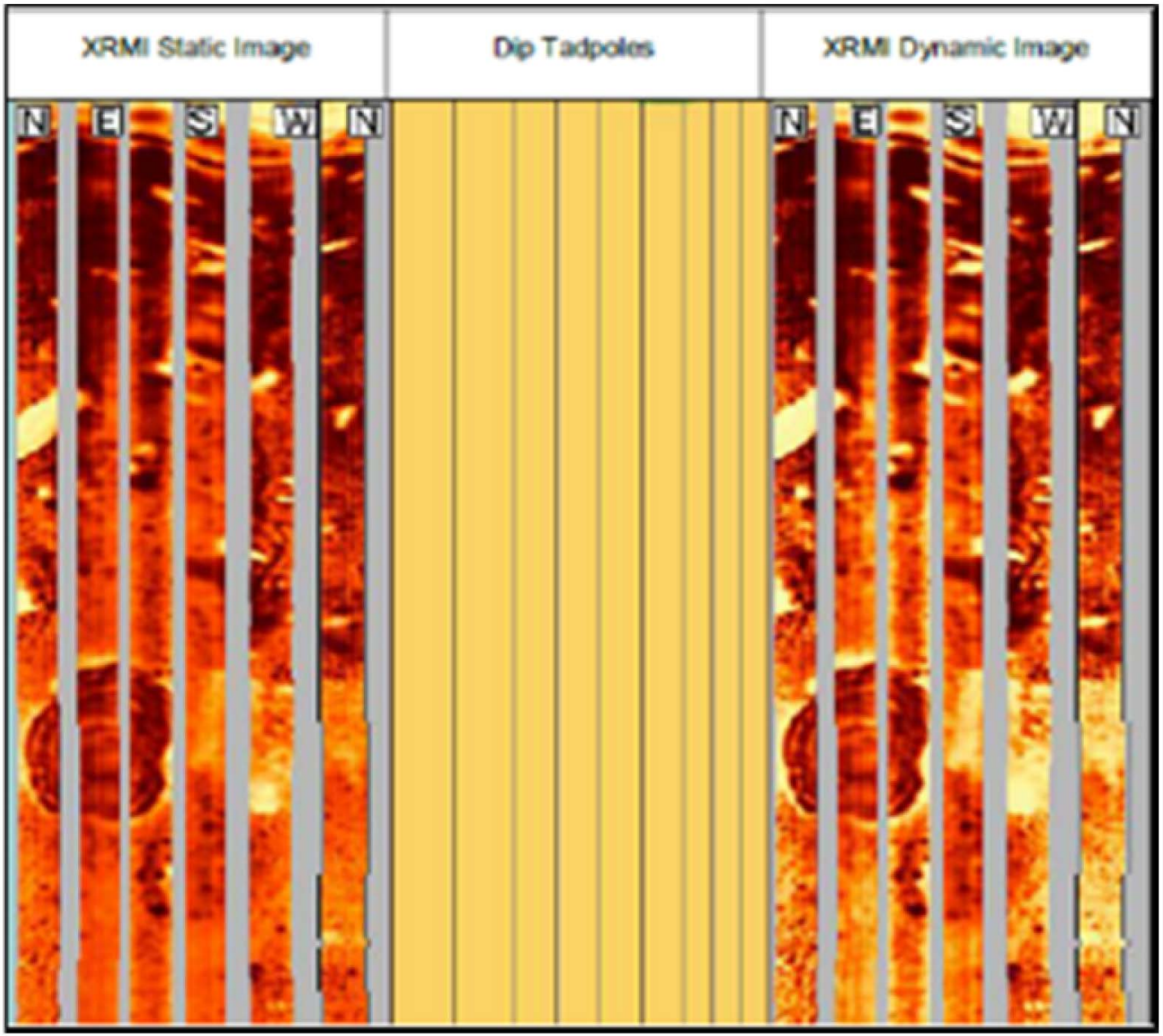

Figure 5. Air fall deposits subfacies.

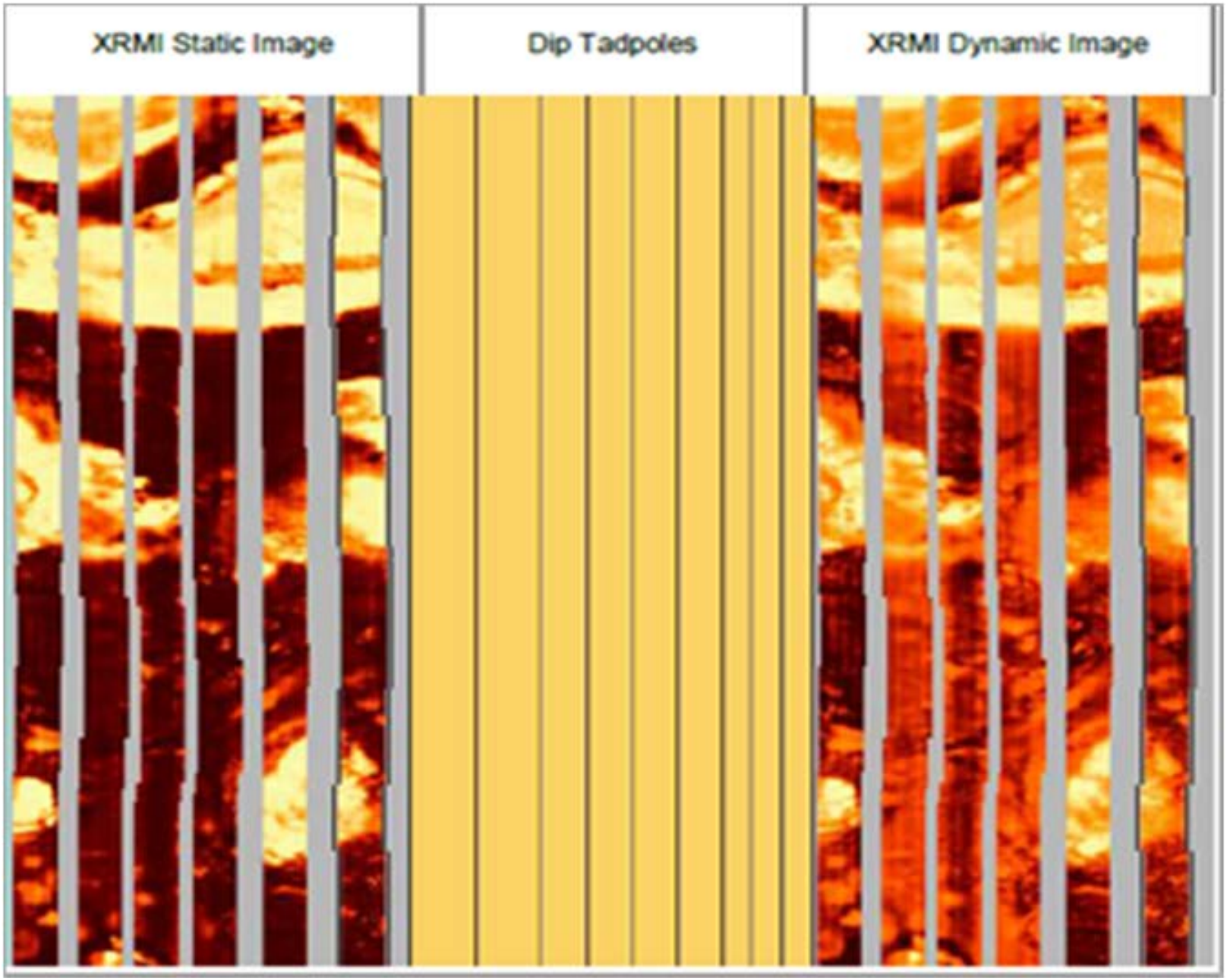

Figure 6. Outer extrusive subfacies.

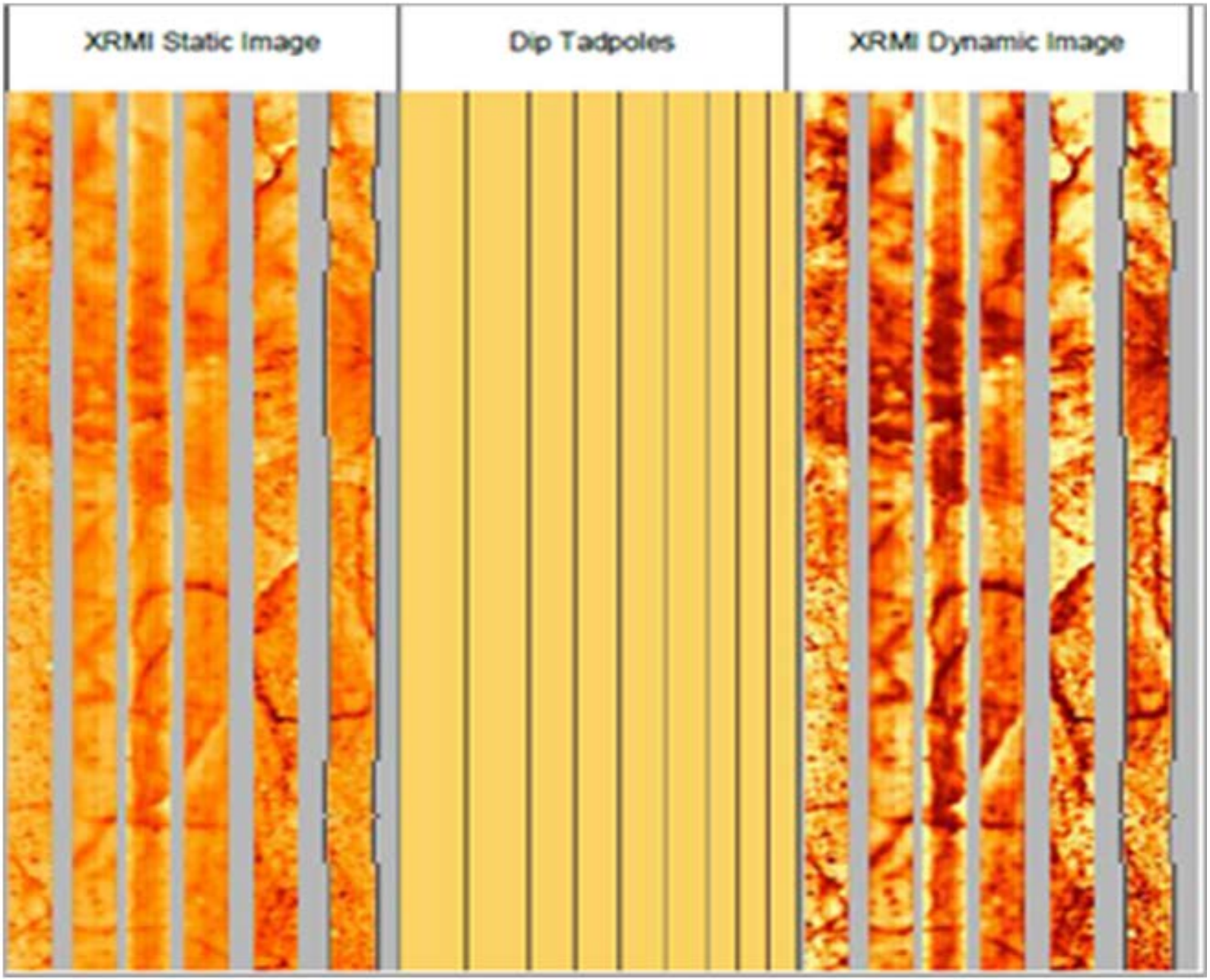

Figure 7. Middle extrusive subfacies.

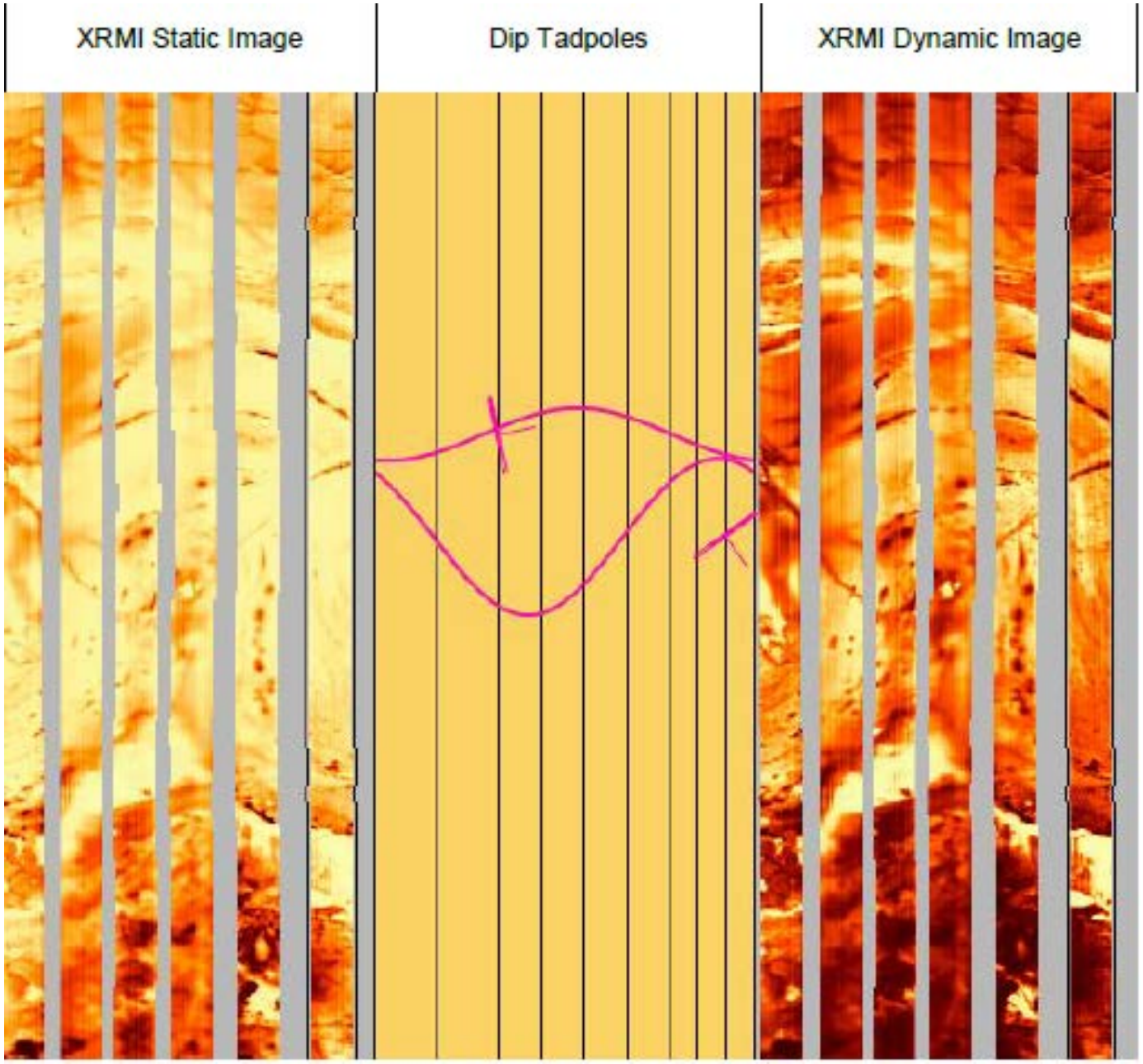

Figure 8. Upper effusive subfacies.

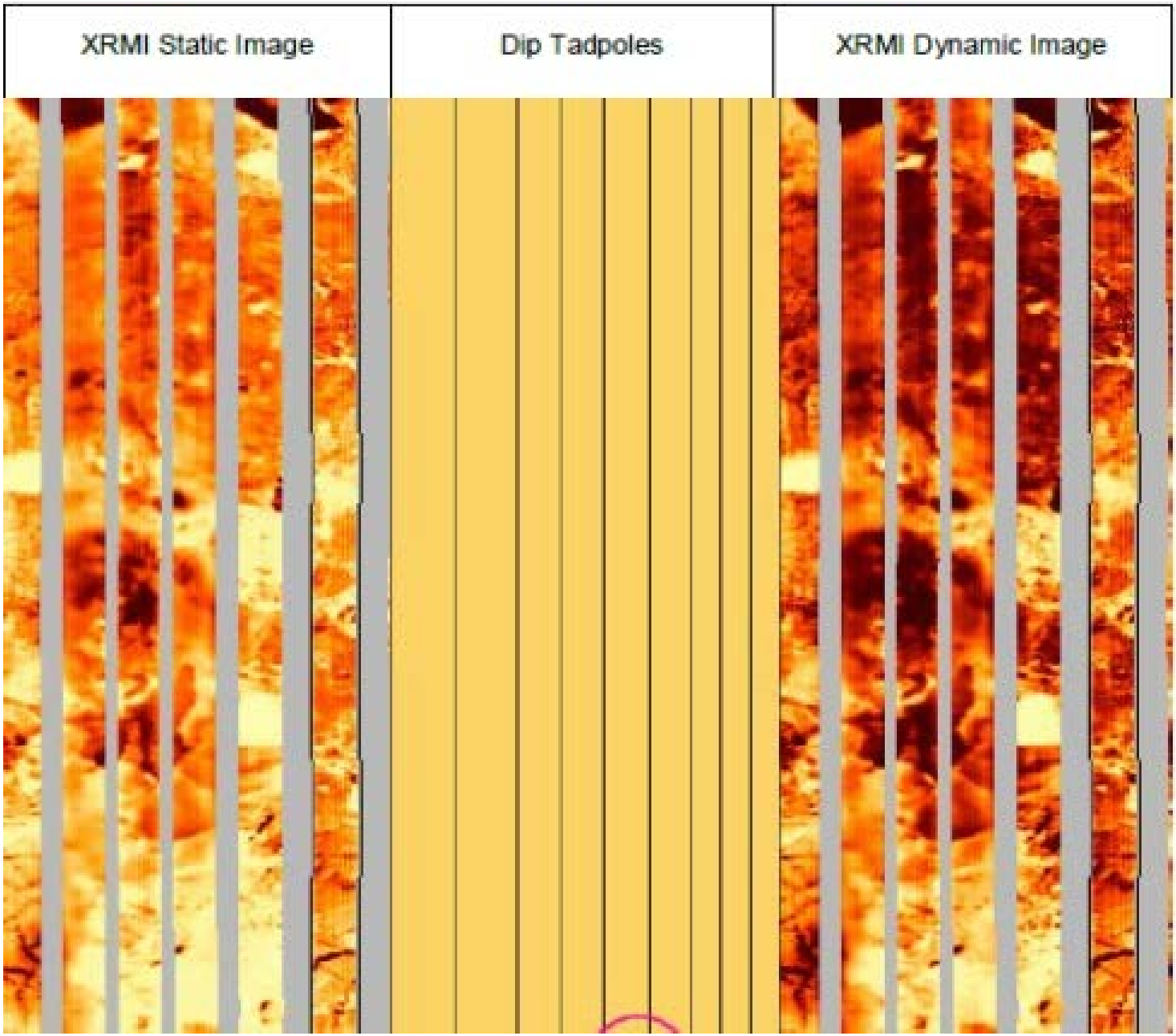

Figure 9. Explosive breccia subfacies.

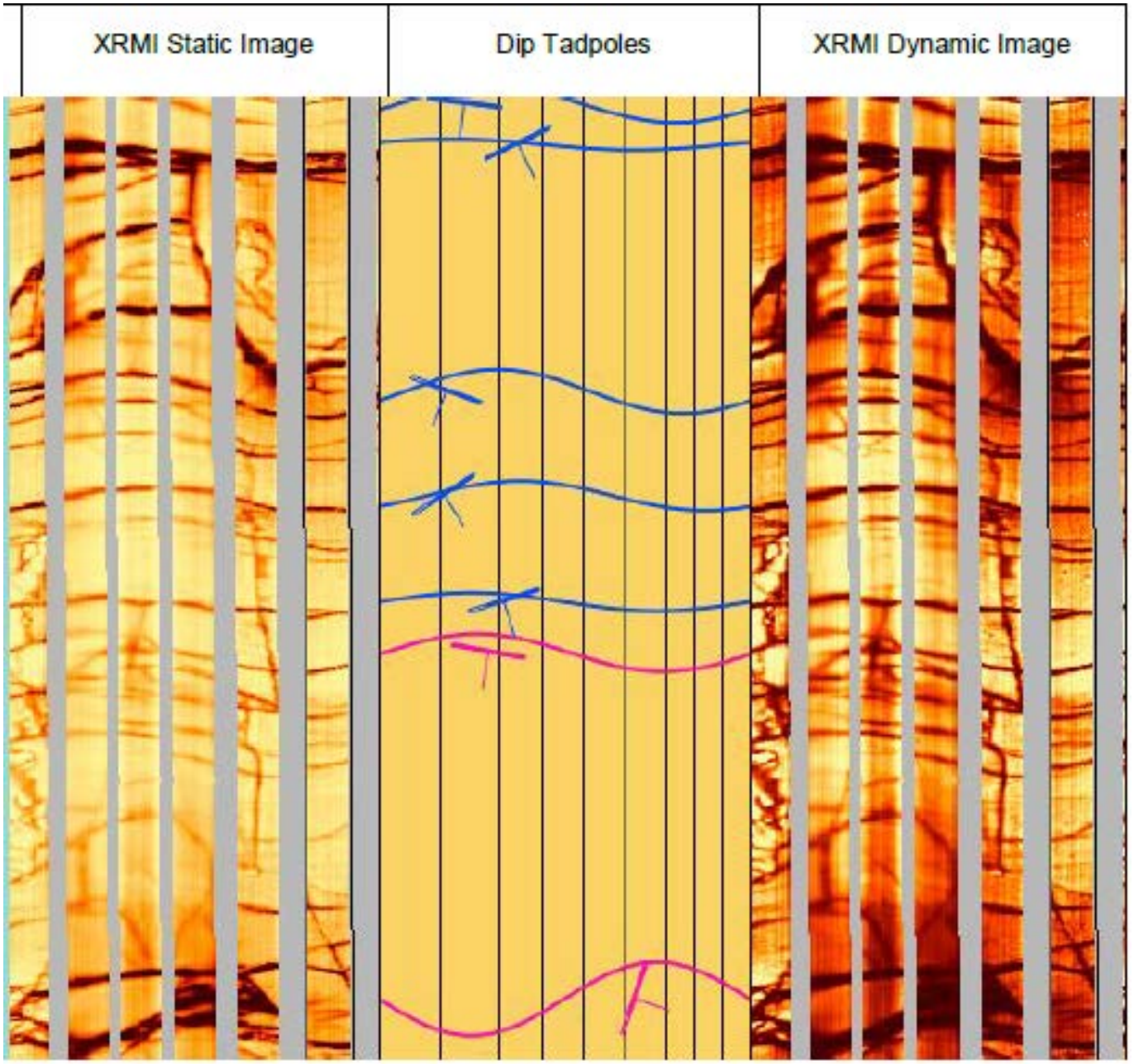

Figure 10. Dike or sill subfacies.

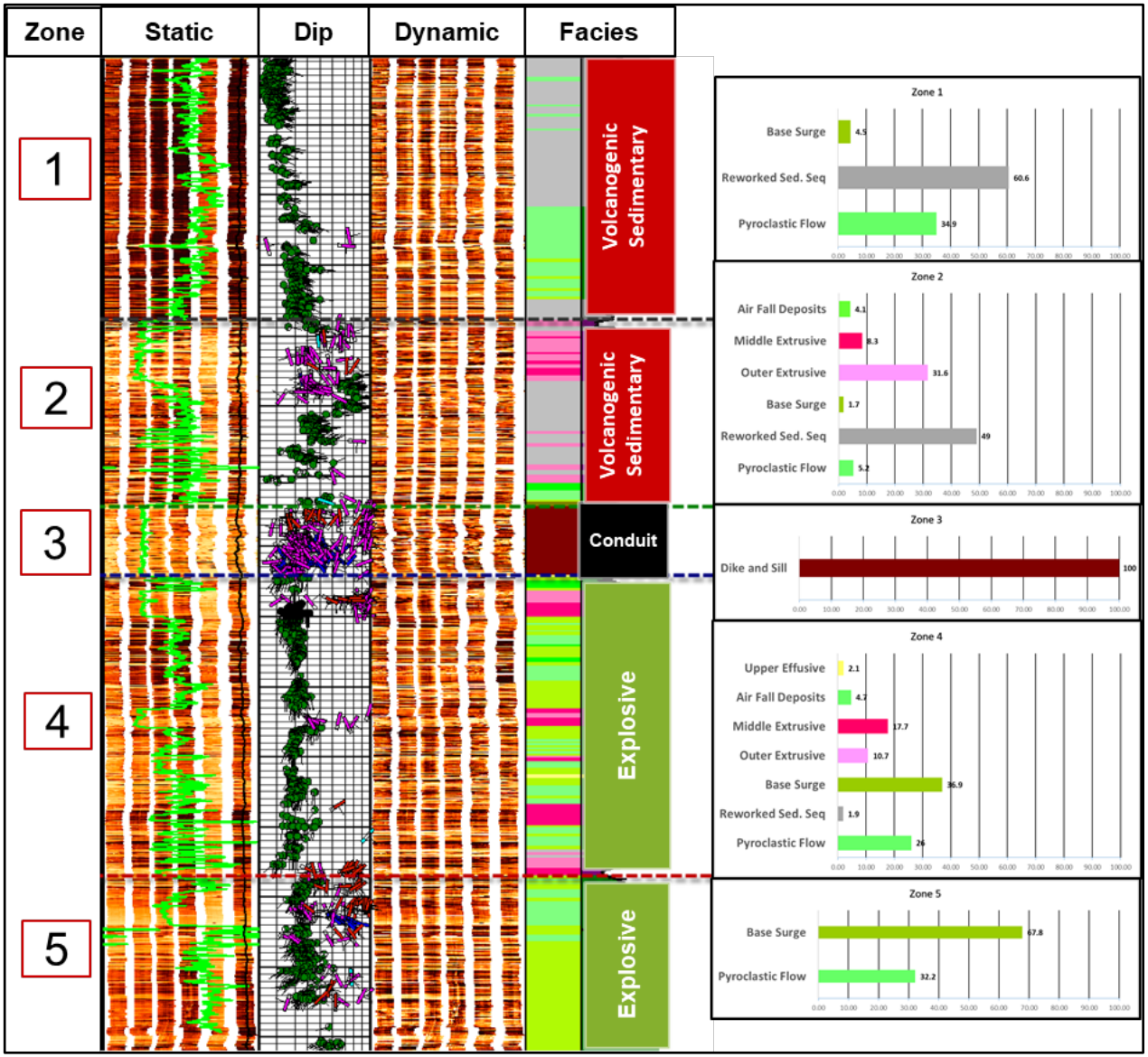

Figure 11. Facies distribution in a volcanic edifice across the study well. Track 1: Static image overlain by gamma ray response (lime green). Track 2: Dip track in which the green tadpole indicates beddings, magenta tadpole indicates partial fracture, red tadpole indicates resistive fracture, and blue tadpole indicates conductive fracture. Track 3: Enhanced dynamic images. Track 4 and Track 5: Subfacies and facies assemblages. The chart on the right shows the percentage of subfacies in each zone.

Geological Age (Ikebe et al., 1977)			Aomori	Akita	Yamagata	Niigata
Quaternary	Holocene		Alluvium Terrace Deposit	Alluvium Terrace Deposit	Alluvium Terrace Deposit	Alluvium Terrace Deposit
	Late Pleistocene		——	Katanishi Fm.	Shohnai Gr.	Oguni Fm.
			Tsurugasaka Fm.	Shibikawa Fm.		Tsukayama Fm. / Wanazu Fm.
	Early Pleistocene		Narusawa Fm.	Sasaoka Fm.	Kannonji Fm.	Haizume Fm.
	Pliocene		Maido Fm.	Upper Tentokuji Fm.	Maruyama Fm.	Nishiyama Fm.
				Lower Tentokuji Fm.	Tateyama Fm.	Hamatsuda Fm.
Neogene	Miocene	Late	Akaishi Fm.	Upper Fnakawa Fm.	Kitamata Fm.	Shiiya Fm. / Araya Fm.
				Lower Fnakawa Fm.		Upper Teradomari Fm.
		Middle	Daidoji Fm.	Onnagawa Fm.	Kusanagi Fm.	Lower Teradomari Fm.
			Tanosawa Fm.	Nishikurosawa Fm.	Aosawa Fm.	Nanatani Fm.
		Early	Sawabe Fm.	Daijima Fm.	Zenpoji Fm.	Tsugawa Fm.
			Iwadate Fm.	Monzen Fm.	Atsumi Gr.	Aikawa Gr.
				Akashima Fm.		

Table 1. Geological correlation of Neogene-Quaternary units in northeastern Honshu, Japan (after Aoyagi and Iijima 1983).

Image Facies	Colors & Patterns	Image Sub-Facies	Colors & Patterns	Image Description
Volcanogenic Sedimentary		Reworked sedimentary		Layered sediments or reworked volcanic sediments. Clear geometry of plane where sinusoid can be fitted in. Evident parallel/cross bedding with consist orientation and magnitude can be observed. Occurrences of calcite streak. May exhibit soft deformation in some interval.
Explosive		Pyroclastic flow		volatile hot mixture with pyroclast and magma flow on surface, may appear as massive or welded materials which may form beddings but appear as distorted planes
		Base surge deposits		Multiple phase of gas, liquid and solid from air ejection forms turbidity flows under gravity on surface, parallel bedding/ cross bedding evident, may appear deformed with indication of parallel beds/ flows, pyroclastic structure may/may not be observed
		Airfall deposits		Falling rock fragments under influence of gravity and air, appears as agglomerate/bombs with different sizes with random orientation
Extrusive		Outer extrusive		Welded breccia and tuff, lava weld new and old rock fragments, with deformed fluidal structure, image shows resistive and conductive angular or rounded fragments patches
		Middle extrusive		Condensation and consolidation of lava, on image appears to be massive unit, fractures and fissures may be observed
Effusive		Upper effusive		Crystals and syn-eruption breccia bearing lava flows on surface under gravity. Breccia appear as mixture of rock fragments cemented together and which may appear as cemented resistive and conductive fragments. Rounded conductive/resistive rounded "bubbles" / (vesicles) may be observed
Conduit facies		Explosive breccia		Volatile magma intrudes and explodes in surrounding rocks, which are then broken and cemented by magma, on image appears to be brecciated with resistive and conductive materials
		Dikes or sills		Magma intrusion, overall massive, appears to be highly resistive on the image, massive with conductive bandings, abundant of fractures and fissures and exhibit brittle texture

Table 2. Image electro-subfacies and facies types with image descriptions (modified from Liu et al. 2012).